atoms

MDPI

Article

Superstructure and Distorted-Wave Codes and Their Applications

Anand K. Bhatia

Heliophysics Science Division, NASA/Goddard Space Flight Center, Greenbelt, MD 20771, USA; anand.k.bhatia@nasa.gov

Abstract: There have been many observations of the solar and astrophysical spectra of various ions. The diagnostics of these observations require atomic data that include energy levels, oscillator strengths, transition rates, and collision strengths. These have been calculated using the Superstructure and Distorted-wave codes. We describe calculations for various ions. We calculate intensity ratios and compare them with observations to infer electron densities and temperatures of solar plasmas.

Keywords: energy levels; oscillator strengths; transition rates; collision strengths; level populations; intensities

check for updates

Citation: Bhatia, A.K. Superstructure and Distorted-Wave Codes and Their Applications. *Atoms* **2022**, *10*, 47. https://doi.org/10.3390/atoms10020047

Academic Editor: Claudio Mendoza

Received: 14 March 2022
Accepted: 28 April 2022
Published: 6 May 2022

1. Introduction

In early 1970s, solar physicists from the solar branch came to talk to Aaron Temkin and me. They showed us Figure 1, having observations of X-ray spectrum from OSO-5, showing emission lines from Si, S, Ar, Ca, Fe, and Ni ions (Neupert [1]). They mentioned that there are many more observations and they do not know how to interpret all the observations to infer parameters of the solar plasma. They would like to know how to calculate electron temperatures, densities, etc., of the solar plasma from the observed intensities of lines. In other words, there were no atomic data available for diagnostic purposes.

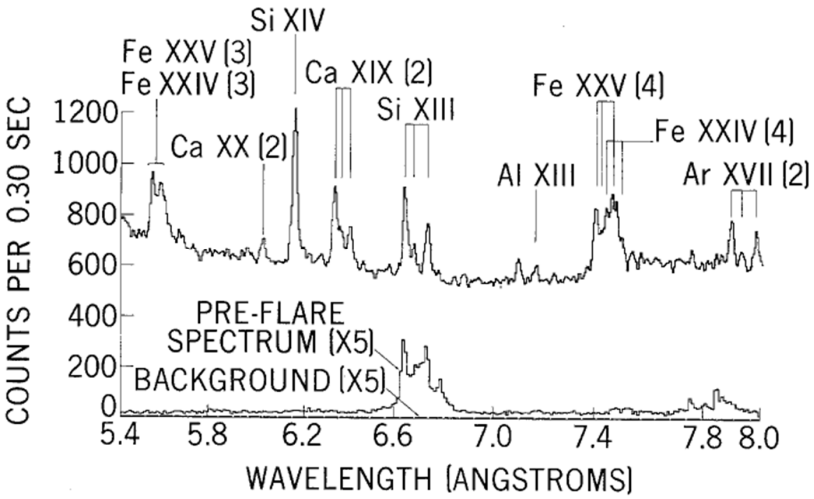

Figure 1. Solar flare spectrum obtained by crystal spectrometer on OSO-5.

We started working on this problem. Temkin and I [2] published 'A distorted-wave methodology for electron-ion excitation: calculations for two-electron ions.' It was clear that a lot more was needed for diagnostics. We needed energies of various levels of the ion, oscillator strengths, transition rates, and excitation cross sections for many, many ions. We could not carry out all the necessary work. It was clear that we needed general computer programs to carry out and analyze observations. We came to know that the Seaton's group at the University College London has developed codes that have all the required

features. We contacted Mike Seaton and he told me to come to the University College and he would try to help. I spent a few days there. I learned there some details about the codes called Super Structure [3], which, using configuration type wave function in the field of the scaled Thomas–Fermi potentials, calculates atomic structure in intermediate coupling, allowing for spin-orbit and radiative and relativistic corrections using Breit–Pauli Hamiltonian as a perturbation to the nonrelativistic Hamiltonian. The target functions are expanded in terms of Slater states. The Thomas–Fermi potentials depend upon parameters λ_i, which are determined variationally. Any other potential could have been used. However, Eissner et al. [3] found that the Thomas–Fermi was the most expedient to use when a large number of energy levels of a target are involved. In addition, inclusions of corrections like hyperfine structure and quantum electrodynamics (QED) corrections are not important. They are too small to affect the accuracy of energies of various levels. We calculated collision strengths for the excitation of Fe XV levels using the Distorted-wave approach as well the R-matrix approach. We find that the Distorted-wave code gives collision strengths that compare well with those obtained from the R-matrix code; atomic data also agree. Atomic data such as energy levels, oscillator strengths, and radiative transition rates are calculated in *LS* and intermediate coupling. Collision strengths are also needed. These are calculated using the Distorted-wave code. The Distorted-wave code [4] treats all the scattering channels as independent, i.e., there is no coupling between the various scattering functions. The scattering function satisfies the equation

$$[\frac{d^2}{dr^2} - \frac{l_i(l_i+1)}{r^2} + \frac{2z}{r} + V_i(r) + k^2]F_i(r) = 0 \quad (1)$$

In the above equation, z = Z − N is the ion charge, Z being the nuclear charge and N the number of electrons, and $V_i(r)$ is a central potential, chosen as Thomas–Fermi potential, the same as used in the superstructure code. The scattering functions satisfy the boundary conditions

$$F_i(0) = 0 \quad (2)$$

$$F_i(r \to \infty) = \frac{1}{k_i^{0.5}} \sin(k_i r - \frac{l_i \pi}{2} + \frac{z}{k_i} \ln(2k_i r) + \arg(\Gamma(l_i + 1 - \frac{iz}{k_i} + \delta_{l_i}), \quad (3)$$

where δ_{l_i} is the phase shift in addition to the Coulomb phase shift. There are a number of excited states of the target, and equations like Equation (1) have to be solved for each case. The reaction matrix is given by

$$K_{ij} = -\langle \Psi_i | H_{N+1} - E | \Psi_i \rangle \quad (4)$$

and T-matrix is given by

$$T = -\frac{-2iK}{1+iK} \quad (5)$$

Collision strength for total angular momentum L, spin S and parity π is

$$\Omega_{ij}^{LS\pi} = \frac{(2L+1)(2S+1)}{2} \sum_{l_i l_j} |T|^2 \quad (6)$$

Total collision strength, symmetric in i and j is given by

$$\Omega_{ij} = \sum_{LS\pi} \Omega_{ij}^{LS\pi} \quad (7)$$

Over the years, we calculated atomic data using Superstructure and Distorted-wave codes for a large number of ions. It is not possible to discuss all of them in this article. We note a few of these ions, not necessary in any particular order.

One of my first publications was with Helen Mason [5] on the carbon sequence: Ar XIII, Si IX, S XI. After this, we [6] calculated atomic data for the nitrogen sequence: Mg VI, Si VIII, S X, A XII, and Ca XIV.

The intensity of a line is given by

$$I_{ji} = N_j A_{ji} \Delta E_{ij} \tag{8}$$

Here I_{ji} is the intensity of the line from the upper level N_j to the lower level N_i, A_{ji} is the transition rate, and ΔE_{ij} is the energy difference between the levels. Knowing the excitation and de-excitation rates, C^e_{ij} and C^d_{ji}, we solve the statistical equilibrium equations for the level populations subject to the condition

$$N = \sum_i N_i \tag{9}$$

$$\frac{dN_i}{dt} = -N_e N_i \sum_{j>i} C^e_{ij} + \sum_{j>i} N_j A_{ji} - N_i \sum_{j<i} A_{ji} + N_e \sum_{j.i} N_j C^d_{ji} \tag{10}$$

This is solved subject to the condition that in the steady state

$$\frac{dN_i}{dt} = 0 \tag{11}$$

The excitation and de-excitation rates are given by

$$C^e_{ij} = \frac{8.63 \times 10^{-6}}{\omega_i k T_e^{1.5}} \int_{\Delta E_{ij}}^{\infty} \Omega_{ij}(E) \exp(-E/kT_e) dE \tag{12}$$

$$C^d_{ji} = \frac{\omega_i}{\omega_j} \exp\left(\frac{\Delta E_{ij}}{kT_e}\right) C^e_{ij} \tag{13}$$

In (12), collision strength $\Omega_{ij} = \omega_i k^2 \sigma_{ij}$ where the excitation cross section σ_{ij} is in πa_0^2 units. Cascades from the upper levels to the lower levels is taken into account by the last term in Equation (10).

In this calculation, we have used configuration interaction, levels arising from these configurations: $2s^2 2p^3$, $2s2p^4$, and $2p^5$ are indicated in Table 1. Energy levels are shown in Table 1.

Table 1. Energies (cm^{-1}) for various ions.

Index	Conf.	State	Mg VI	Si VIII	S X	AXII	Ca XIV
1	$2s^2 2p^3$	$^4S_{1.5}$	0	0	0	0	0
2		$^2D_{1.5}$	58,192	72,029	85,285	97,597	108,642
3		$^2D_{2.5}$	58,196	72,351	86,613	101,272	116,780
4		$^2P_{0.5}$	82,514	103,847	125,416	147,556	170,748
5		$^2P_{1.5}$	82,592	104,374	127,280	152,547	181,829
6	$2s2p^4$	$^4P_{2.5}$	246,690	311,146	376,762	444,085	513,787
7		$^4P_{1.5}$	248,257	314,588	383,415	455,831	533,168
8		$^4P_{0.5}$	249,167	316,533	387,030	461,887	542,478
9		$^2D_{1.5}$	351,770	440,103	530,170	622,911	719,373
10		$^2D_{2.5}$	351,800	440,220	530,537	623,886	721,656
11		$^2S_{0.5}$	409,970	512,310	616,130	722,250	811,587
12		$^2P_{1.5}$	443,017	548,033	654,192	762,566	874,454
13		$^2P_{0.5}$	444,934	552,325	662,704	778,054	960,767

For scattering functions, we used seven partial waves for the incoming electron. We used Coulomb Bethe approximation for the higher partial waves. The transition rates and collision strengths at incident energies 15, 30, and 45 Ry are given in Table 2 for Ca XIV; we do not give here collision strengths for other ions given in [6].

Table 2. Radiative rates (s^{-1}) and collision strengths at various incident energies (Ry) for Ca XIV.

Transition	A_{ji}	Collision Strengths		
		15	**30**	**45**
1-2	5.28 (2)	0.0643	0.0457	0.0340
1-3	1.47 (1)	0.0785	0.0568	0.0430
1-4	1.57 (3)	0.0224	0.0148	0.0103
1-5	2.91 (3)	0.0372	0.0250	0.0176
1-6	8.65 (9)	0.9188	1.0289	1.1140
1-7	9.72 (9)	0.6020	0.6753	0.7327
1-8	1.04 (10)	0.3130	0.3470	0.3743
1-9	3.67 (7)	0.0015	0.0011	0.0009
1-10	1.72 (6)	0.0003	0.0002	0.0001
1-11	1.78 (8)	0.0026	0.0021	0.0017
1-12	4.93 (8)	0.0217	0.0185	0.0162
1-13	7.95 (6)	0.0082	0.0060	0.0046
2-3	5.07	0.0943	0.0708	0.0561
2-4	5.33 (2)	0.0456	0.0427	0.0414
2-5	1.35 (3)	0.0476	0.0396	0.0349
2-6	2.87 (7)	0.0143	0.0113	0.0092
2-7	6.71 (5)	0.0131	0.0096	0.0073
2-8	1.27 (7)	0.0075	0.0055	0.0042
2-9	2.25 (10)	0.8940	0.9966	1.0780
2-10	1.20 (8)	0.0223	0.0175	0.0141
2-11	1.51 (10)	0.1731	0.1915	0.2065
2-12	1.31 (10)	0.2359	0.2682	0.2913
2-13	3.88 (10)	0.3209	0.3576	0.3871
3-4	2.87 (−1)	0.0434	0.0383	0.0355
3-5	5.73 (2)	0.1084	0.1004	0.0962
3-6	3.30 (7)	0.0285	0.0225	0.0181
3-7	2.91 (6)	0.0099	0.0074	0.0057
3-8		0.0014	0.0010	0.0008
3-9	8.73 (8)	0.0551	0.0543	0.0545
3-10	1.99 (10)	1.1946	1.3416	1.4380
3-11		0.0005	0.0003	0.0002
3-12	6.58 (10)	1.2597	1.4010	1.5163
3-13		0.0026	0.0019	0.0014
4-5	1.07 (1)	0.0480	0.0357	0.0280
4-6		0.0029	0.0022	0.0017

Table 2. *Cont.*

Transition	A_{ji}	Collision Strengths		
		15	**30**	**45**
4-7	2.16 (5)	0.0082	0.0060	0.0045
4-8	1.59 (7)	0.0081	0.0061	0.0047
4-9	2.42 (9)	0.1461	0.1604	0.1717
4-10		0.0084	0.0064	0.0049
4-11	2.15 (10)	0.3459	0.3812	0.4088
4-12	4.45 (9)	0.1142	0.1302	0.1357
4-13	6.75 (9)	0.0741	0.0829	0.0898
5-6	9.92 (6)	0.0121	0.0095	0.0076
5-7	3.03 (7)	0.0177	0.0136	0.0108
5-8	3.47 (2)	0.0080	0.0059	0.0045
5-9	2.01 (8)	0.0197	0.0157	0.0129
5-10	4.13 (9)	0.3773	0.4204	0.4539
5-11	1.19 (10)	0.2091	0.2265	0.2412
5-12	9.28 (9)	0.2409	0.2692	0.2913
5-13	4.51 (10)	0.5212	0.5802	0.6272

Level populations of the first five levels are given in Table 3, and intensity ratios are given in Table 4, where we have used wavelengths given by Kelly and Palumbo [7].

Table 3. N_i/N for various electron densities N_e (cm^{-3}) for Ca XIV.

Level	10^8	10^9	10^{10}	10^{11}	10^{12}
1	1.0	1.0	0.96	0.86	0.68
2	0.24 (−4)	0.24 (−3)	0.24 (−2)	0.21 (−1)	0.10
3	0.53 (−3)	0.51 (−2)	0.39 (−1)	0.12	0.19
4	0.12 (−5)	0.13 (−4)	0.14 (−3)	0.16 (−2)	0.17 (−1)
5	0.96 (−6)	0.99 (−5)	0.12 (−3)	0.17 (−2)	0.20 (−1)

Table 4. Intensity ratios relative to transition 1-6 for N_e (cm^{-3}) for Ca XIV.

Transition	λ(Å)	Electron Density (cm^{-3})				
		10^8	10^9	10^{10}	10^{11}	10^{11}
1-6	193.88	1.0	1.0	1.0	1.0	1.0
1-7	186.02	0.68	0.68	0.68	0.68	0.68
1-8	183.46	0.36	0.36	0.36	0.36	0.36
2-9	165.36	0.00	0.00	0.00	0.03	0.16
3-10	167.00	0.00	0.00	0.03	0.11	0.24
3-12	134.30	0.02	0.02	0.05	0.14	0.30

Below, we discuss atomic data and comparison with observations for various ions.

2. O IV and Mg VIII

Observations of solar flares on 9 August–7 September 1973 were obtained by Naval Research Laboratory's SO82B spectrograph on board Skylab, covering the 960–1600 Å wavelength range. Spectra of allowed and intersystem lines of O IV could be observed.

These lines are density sensitive. Cook, Keenan, and Bhatia [8], using configurations $2s^2 2p$, $2s2p^2$, and $2p^3$ calculated the atomic data for O IV to analyze these observations.

The lines at 1342 and 1338.61 Å due to transitions $2p^3\ ^2D_{3/2} \rightarrow 2s2p^2\ \ ^2P_{3/2,1/2}$ should be in the ratio of transition rates because they have the same upper level. However, the calculated ratio was not expected to agree with the observed value because of the contamination of H_2 lines at 1342.88 and 1338.57 Å.

However, the intensity ratio of the allowed line at 1343.51 Å due to the transition $2p^3\ ^2D_{5/2} \rightarrow 2s2p^2\ ^2P_{3/2}$ and the intercombination line at 1407.39 Å due to the transition $2s2p^2\ ^4P_{1/2} \rightarrow 2s^2 2p\ ^2P_{3/2}$ were found to be density sensitive but not temperature sensitive. The observed ratio in the two flares is 0.89 and 0.90, giving an electron density of 1.6×10^{12} cm^{-3} at log(T_{max}) = 5.2, where T_{max} is the temperature of maximum abundance of O IV.

EUV spectral lines of Mg VIII from the solar corona have been observed by Skylab, Solar EUV Rocket Telescope and Spectrographs (SERTS), and also by Solar and Heliospheric Observatory (SOHO). Bhatia and Thomas [9] carried out calculations using configurations $2s^2 2p$, $2s2p^2$, $2p^3$, $2s^2 3s$, $2s^2 3p$, and $2s^2 3d$. These configurations give rise to 20 fine-structure levels. Collision strengths are calculated at incident energies of 15.0, 22.5, 30.0, and 37.5, 45 Ry. The temperature of maximum abundance is log(T_{max}) = 5.9. The calculated intensity ratio I(313.74)/I(317.01) = 1.69 agrees well with the observed value 1.40. These lines originate from the same upper level. Therefore, the ratio depends only on transition rates. The agreement indicates that the calculated radiative rates are reliable. The intensity ratio I(436.73)/I(430.44) is density sensitive and at $N_e = 10^{9.2}$ cm^{-3}, its value is 1.68, which is also the observed value. The inclusion of three more configurations does not change the results.

3. Fe XXI and OIII

The Fe ions are most abundant in the solar atmosphere. Fe XXI has emission lines in the ranges 1–25, 90–200, and 300–2500 Å. Many of these lines have been used for electron density diagnostics. Mason et al. [10] calculated the atomic data using configurations $2s^2 2p^2$, and $2p^4$. The first 5 levels are $^3P_0$, $^3P_1$, $^3P_2$, $^1D_2$, and $^1S_0$ The temperature of maximum abundance is $T_e = 10^7$ K. The calculated intensity ratios of various lines are shown in Table 5.

Table 5. Intensity ratios as a function of electron density.

λ (Å)	log(N_e (cm^{-3}))						
	11.0	**11.5**	**12.0**	**12.5**	**13.0**	**14.0**	**15.0**
142.14	0.013	0.023	0.055	0.147	0.379	1.246	1.465
128.73	1.000	1.000	1.000	1.000	1.000	1.000	1.000
121.22	0.015	0.044	0.118	0.271	0.538	1.422	1.836
102.23	0.228	0.254	0.321	0.469	0.753	1.720	2.144
97.89	0.099	0.110	0.139	0.204	0.327	0.747	0.930

We can understand the sensitivity of lines at 142.14 and 128.73 Å due to transitions $2s2p^3\ ^3D_2 \rightarrow 2s^2 2p^2\ ^3P_1$ and $2s2p^3\ ^3D_1 \rightarrow 2s^2 2p^2\ ^3P_0$, respectively. The level $^3D_1$ is populated from the ground level $^3P_0$, which is more populated than the level $^3P_1$, resulting in the higher intensity for line at 128.73 Å. Fractional level populations are given in Table 6.

Table 6. Populations of levels in the ground configuration as a function electron density.

Level	11.0	11.5	12.0	12.5	13.0	14.0	15.0
$^3P_0$	9.97 (−1)	9.06 (−1)	7.75 (−1)	5.80 (−1)	3.77 (−1)	1.45 (−1)	9.84 (−2)
$^3P_1$	7.40 (−3)	2.17 (−2)	5.73 (−2)	1.27 (−1)	2.25 (−1)	3.05 (−1)	2.52 (−1)
$^3P_2$	2.56 (−2)	7.16 (−2)	1.66 (−1)	2.86 (−1)	3.71 (−1)	3.95 (−1)	3.68 (−1)
$^1D_2$	9.72 (−5)	3.86 (−4)	1.73 (−3)	7.44 (−3)	2.65 (−2)	1.42 (−1)	2.45 (−1)
$^1S_0$	5.34 (−6)	1.84 (−5)	6.90 (−5)	2.73 (−4)	1.10 (−3)	1.34 (−2)	3.72 (−2)

O III atomic data have been calculated by Bhatia and Kastner [11]. This ion is particularly important because the He II 303.8 Å resonance line coincides with the energy difference between the $2s^22p^2\,{}^3P_2$ and $2s^22p3d\,{}^3P_2$ levels. Therefore, the upper level is excited by He II from the lower level, producing a fluorescent cascade of visible and ultraviolet lines due to the decay of the photoexcited level. This cascade is through the levels of $2p3p$ and $2p3s$ configurations. This is known as the Bowen fluorescence mechanism (Bhatia, Kastner, and Behring [12]). The statistical equations are solved in the presence of the He II radiation field to obtain level populations and then intensities using Equation (8). A convincing proof of the Bowen mechanism comes from the fact that the 303.63 Å line in the spectra of the Sun obtained by Behring et al. [13] and the multiplet at 644 Å in the Skylab spectra obtained by Vernazza and Reeves [14] would not have been seen. Furthermore, the calculated intensity of the multiplet at 644 Å in the presence of photoexcitation agrees with the observed intensity. The primary cascade lines originating from $2p3d\,{}^2P_2$ to the levels of 2p3p are 3444.10, 3132.84, 2837.17, and 2819.57 Å, and the secondary cascade lines between the levels of 2p3p and 2p3s are 3759.87, 3340.75, 3312.30, 3299.36, 3047.13, and 3023.45 Å (Kastner et al. [15]).

The ratio I(3444)/I(5007) in planetary nebulae can be used to infer the photoexcitation rates P of the He II resonance line, 3444 Å line is due to the transition $2s^22p3d\,{}^3P_2 \rightarrow 2s^22p3p\,{}^3P_2$, being a Bowen line, and 5007 Å line is a forbidden non-Bowen line $2s^22p^2({}^1D_2 \rightarrow {}_3P_2)$. Having established P, the electron density can be determined from density sensitive infrared line ratio I(88.3 μm)/I(51.8 μm). The line at 88.3 μm is due to $2s^22p^2({}^3P_1 \rightarrow {}_3P_0)$, and the 51.8 μm line is due to $2s^22p^2({}^3P_2 \rightarrow {}_3P_1)$. As $^3P_2$ is the upper level of the 51.8 μm line and the lower level of the pumped transition, the ratio is sensitive to P as well as to N_e, which can both be determined by comparing intensity ratios with observations (Bhatia and Kastner [16]).

There are other examples of the Bowen mechanism. The O III 374.436 Å line due to the transition $2s^22p3s\,{}^3P_1 \rightarrow 2s^22p^2\,{}^3P_2$ can photoexcite the level in N III, giving 374.441 Å and 374.434 Å lines, but a comparison with solar and nebular observations indicates that this process plays a small role, unlike in O III. The quenching of the infrared 57.3 μm line, emitted in the ground configuration transition $2s^22p({}^2P_{3/2} \rightarrow {}_2P_{1/2})$, is due to photoexcitation from the $2s^22p\,{}^2P_{3/2}$ level to $2s^23d\,{}^2D_{3/2,5/2}$ levels. This shows the presence of the Bowen mechanism (Kastner and Bhatia [17]). There are number of ions for which the Bowen mechanism is possible (Kastner and Bhatia [18]).

4. X-ray Lines from Fe XXI and Fe XXII

The Fe XXI emission lines in the 9.5–9.8 Å range were observed during an intense flare on 2 July 1985 with the Flat Crystal Spectrometer on the Solar Maximum Mission satellite (SMM) (Fawcett et al. [19]). To determine electron densities, Phillips et al. [20] carried out calculations using configurations $2s^22p^2$, $2s2p^3$, $2p^4$, $2s^22p4s$, $2s^22p4d$, $2s^22p5s$, $2s^22p5d$, giving rise to 42 fine-structure levels. Transitions for these X-ray lines with their wavelengths, radiative rates, and collision strengths at three incident energies of 110, 220, and 330 Ry are given in Table 7.

Table 7. Atomic data for Fe XXI X-ray lines.

Trans. (i-j)	λ (Å)	A_{ji} (s^{-1})	Ω (110)	Ω (220)	Ω (330)
1-28	9.476	6.37 (12)	0.0091	0.0150	0.0187
2-26	9.546	4.88 (12)	0.0132	0.0202	0.0250
2-28	9.541	9.91 (11)	0.0028	0.0027	0.0031
2-30	9.457	1.95 (12)	0.0051	0.0077	0.0095
3-37	9.585	3.67 (12)	0.0151	0.0215	0.0265
3-31	9.489	5.73 (12)	0.0201	0.0318	0.0397

Oscillator strengths are not given in the above table. However, they can be obtained from the relation between oscillator strengths and transition rates given below:

$$A_{ji} = \frac{6.670 \times 10^{15} \omega_i f_{ij}}{\lambda^2 \omega_j} \tag{14}$$

The calculated intensity ratios are compared with observations in Table 8.

Table 8. Observed and theoretical wavelengths and intensities for Fe XXI.

Observed Intensity Ratios				Calculated				
Lett.	λ (Å)	Trans.	Intensity Ratio	λ (Å)	Trans.	Log (N_e)		
						11	12	13
A	9.455	-	0.080	9.457	2-30	0.003	0.014	0.087
B	9.476	1.28	1.000	9.476	1-28	1.001	1.005	1.032
C	9.482	2.31	0.163	9.489	3-31	0.015	0.088	0.408
D	9.542	2.28	0.138	9.541	2-28	0.155	0.155	0.159
E	9.548	2.30	0.146	9.546	2-26	0.100	0.133	0.370
F	9.587	3.27	0.080	9.585	3-37	0.078	0.127	0.346

The relative observed intensities of lines C and E agree well with the theoretical intensities at N_e more than 10^{12} cm^{-3}. The fact that the electron densities in a flare can be so high is also borne out by Fe XXII lines at 8976 Å (P) and 9073 Å (Q and R) observed by SMM FCS (Fawcett et al. [19] and Phillips et al. [20])). The line P is due to the transition $2s^2 4d\,^2D_{3/2} \rightarrow 2s^2 2p\,^2P_{1/2}$, the line Q due to the transition $2s^2 4d\,^2D_{5/2} \rightarrow 2s^2 2p\,^2P_{3/2}$, and the line R due to the transition $2s^2 4d\,^2D_{3/2} \rightarrow 2s^2 2p\,^2P_{3/2}$. These lines are not blended with other lines. The observed intensity ratio [I(Q) + I(R)]/I(P) = 0.54 ± 0.03. Mason and Storey [21] calculated atomic data and concluded that $N_e = 10^{13}$ cm^{-3}.

Atomic data and spectral line intensities for the carbon isoelectronic sequence (Ar XIII through Kr XXXI) using $2s^2 2p^2$, $2s 2p^3$, $2p^4$, $2s^2 2p 3s$, $2s^2 2p 3p$, *and* $2s^2 2p 3d$ configurations are given by Bhatia et al. [22].

5. Mg VI

Eight lines of Mg VI in the EUV range have been identified in the Solar Extreme Ultraviolet Rocket Telescope and Spectrograph (SERTS-89) data (Thomas and Neupert [23]). Bhatia and Mason [6] extended their earlier calculations and calculated atomic data using configurations $2s^2 2p^3$, $2s 2p^4$, $2p^5$, and $2s^2 2p^2 3s$. Collision strengths were calculated at incident energies 7, 10, 35, 50, and 55 Ry for incident partial waves up to 19. Proton rates were also included. Intensities were calculated for log N_e (cm^{-3}) = 8, 10, 12 and log (T_e) = 5.45, 5.60, and 5.73 K.

The model predicts lines at 387.77, 387.93, and 388.00 Å, which is the most intense of these three, the line observed at 387.955 Å is identified with the predicted 388.00 Å due to the transition $2s2p^4\,^2D_{1/2} \rightarrow 2s^2 2p^3\,^2P_{3/2}$. The line observed at 349.162 is identified as a blend of the four predicted lines at 349.11, 349.12, 349.16, and 349.18 Å. Similarly, the observed line at 270.401 Å is identified with a blend of 270.39 and 270.40 Å. The observed intensity ratio I(399.275)/I(403.296) agrees with the predicted intensity ratio. The observed X-ray lines (Behring et al. [13]) are 111.557 and 111.724 Å; the fact that 111.557 Å is the strongest of the two is in agreement with the inference of the calculation.

6. Ne IV

Atomic data for Ne IV have been calculated by Bhatia and Kastner [24] using configurations $2s^2 2p^3$, $2s2p^4$, $2p^5$, $2s^2 2p^2 3s$, $2s^2 2p^2 3p$, and $2s^2 2p^2 3d$, giving rise to 72 fine-structure levels. Multiplets at 358.7, 421.6, and 469.8 Å at $T_e = 10^{5.5}$ K are found to be density sensitive, as shown in Figure 2. The dashed curve represents multiplet 421.6 Å at $T_e = 10^{6.6}$ K. The Bowen mechanism is possible in this ion because of excitation by a coincident wavelength of Fe XI.

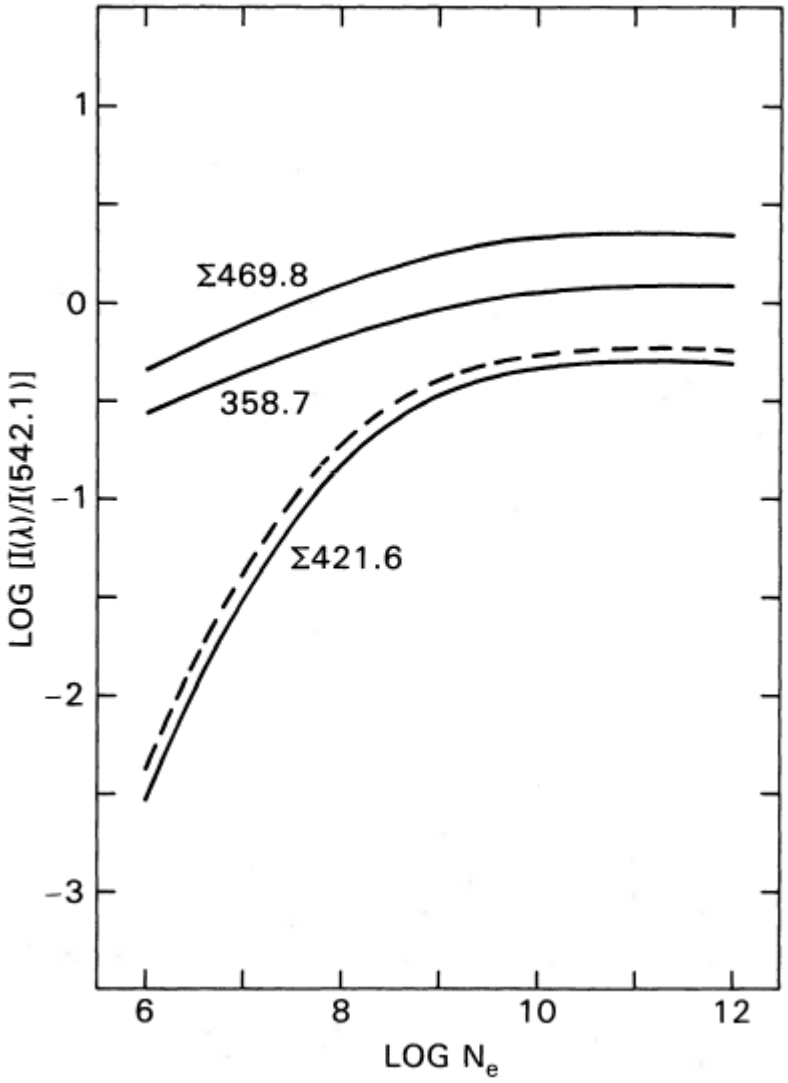

Figure 2. Density sensitive multiplets of N IV.

7. Fe XVII and Resonance Scattering

Neon-like Fe is present in solar flares and solar active regions in a broad temperature range $(2 - 10) \times 10^6$ K. Strong resonance lines in the range 15–17 Å have been

observed by McKenzie et al. [25] and Phillips et al. [26]. The transitions of interest are $2s^2 2p^5 3d\,^1P_1 \rightarrow 2s^2 2p^6\,^1S_0$ at 15.02 Å and $2s^2 2p^5 3d\,^2D_1 \rightarrow 2s^2 2p^6\,^1S_0$ at 15.26 Å along with subordinate lines in the extreme-ultraviolet (EUV) region. There have been a number of theoretical studies of the expected spectrum assuming optically thin conditions. Bhatia and Doschek [27] carried out calculations using seven configurations $2s^2 2p^6$, $2s^2 2p^5 3s$, $2s^2 2p^5 3p$, $2s^2 2p^5 3d$, $2s 2p^6 3s$, $2s 2p^6 3p$, and $2s 2p^6 3d$, giving rise to 37 fine-structure levels. Collision strengths were calculated at five incident energies: 76.83, 92.53, 120.93, 179.73, and 253.23 Ry. Level populations and intensity ratios were calculated as a function of electron density and temperature. The excited states in Fe XVII are much higher than the ground state. The EUV lines have been observed in solar flares recorded by a slitless spectrograph flown on the Skylab manned space station in 1973 (Feldman et al. [28] and Doschek, Feldman, and Bhatia [29]). The calculated relative intensities of lines at $N_e = 10^{11}$ cm^{-3} and $T_e = 4 \times 10^6$ K agreed well with the observed relative intensities [29].

For optically thin plasma, the calculated ratio I(15.02)/I(15.26) = 4.8 whereas the observed ratio is 2.75 ± 0.7 [25,26], and the experimental result of Brown et al. [30] using Electron Ion Beam Trap (EBIT) is 3.04 ± 0.12. Where the calculated intensities do not agree with the observed ones, it seems they suffer resonance scattering, as suggested by Rugge and McKenzie [31]. Resonance scattering implies that the emitted photons are absorbed and reemitted but not necessarily in the line of sight of the observer. There are many other measurements: laboratory measurements of Beierdorfer et al. [32] agree with the satellite measurements of the Sun and they disagree with the assertions that other processes play a role in the formation of Fe XVII spectra. Line intensity ratios given by Laming et al. [33] in their Table 1 are higher than those obtained in DW as well as those obtained in the R-matrix calculations. It should be pointed out that the two calculations give the same results for intensity rations. Bernitt et al. [34] indicate that the poor agreement between the calculations and observations is due to the underlying atomic wave functions rather than insufficient modelling. Therefore, there is a resonance scattering in solar active regions and flares, resulting in an apparent loss of flux, although the total flux integrated over 4π remains unchanged. Optical depth effects have been taken into account, using various approximate treatments, e.g., Rugge et al. [31], Phillips et al. [35], and Saba et al. [36], to interpret observations of the disk center to limb intensity variation. Saba et al. [36] used the escape probability method of Kastner and Kastner [37] and concluded that the intensity of the line 15.02 Å is a factor of 2 to 3 lower than the predicted optically thin value, even though the results are consistent at 15.26, 16.78, and 17.05 Å, but not at 15.02 and 17.05 Å. It is very unlikely that other processes will remove the discrepancy between observations and calculations.

In the recent publication by Kühn et al. [38], theoretical calculation of the ratio $R = f_{3C}/f_{3D}$ of the oscillator strengths of the resonance line 3C at 15.02 Å and the intercombination line 3D at 12.26 Å are given. The theoretically determined R = 3.55 ± 0.02 by a calculation using 1.2 million configurations and over 100 million slater determinants, whereas the experimentally determined R = 3.51 ± 0.02 used EBIT. This is an excellent agreement between theory and experiment. However, these authors have not determined the intensity ratio of these lines, theoretically or experimentally.

Optical depth τ_0, level population N_1, column length L are given [36] in terms of the oscillator strength by

$$\frac{\tau_0}{N_1 L} = 4.35 \times 10^{-17} f \lambda \tag{15}$$

Table 9 from Bhatia and Kastner [39] gives λ, f, A, and $\tau_0/N_1 L$ for transitions originating from $3s$, $3p$, and $3d$ levels at $T_e = 4 \times 10^6$ K.

Table 9. Fe XVII resonance lines and forbidden line at 17.10 Å.

Upper Level	λ (Å)	*F*	*A* (s^{-1})	$\tau_{0/N_1 L}$
$2p^5 3s\,^3P_2$	17.10	4 (−8)	1.60 (5)	0.0
$2p^5 3s\,^1P_1$	17.05	0.123	9.44 (5)	7.50 (−17)
$2p^5 3s\,^3P_1$	16.78	0.101	8.00 (11)	8.08 (−17)
$2p^5 3d\,^3P_1$	15.45	0.089	8.27 (10)	5.96 (−18)
$2p^5 3d\,^3D_1$	15.26	0.593	5.69 (12)	3.94 (−16)
$2p^5 3d\,^1P_1$	15.02	2.662	2.64 (13)	1.74 (−15)
$3s^2 p^5 3p\,^1P_1$	13.82	0.275	3.21 (12)	1.66 (−16)

These studies indicate that the strongest line at 15.02 Å can have significant optical depth. It is found that the upper level $2p^5 3d\,^1P_1$ of the most optically thick resonance line is at 15.02 Å at $T_e = 4 \times 10^6$ K and for $N_e = 10^9$, 10^{10}, and 10^{11} cm^{-3}, as shown Figure 3 taken from Bhatia and Kastner [39].

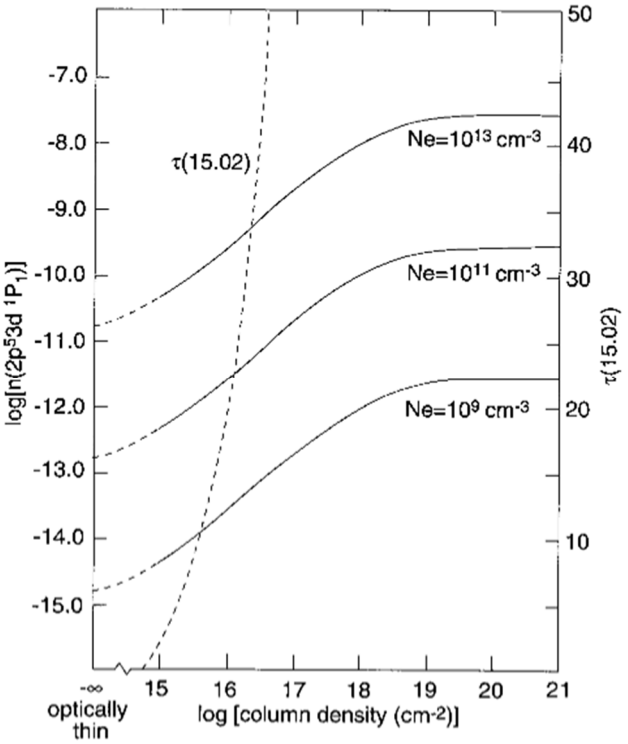

Figure 3. Variation of the population of upper level $3p^5 3d\,^1P_1$ of the 15.02 Å resonance line, with increasing column density of Fe XVII.

The level population increases by a factor of 1000 at a column length of 10^{21} cm^{-2} compared to the optically thin value. All the EUV lines originating from 3d levels are also affected by the opacity [40]. Eleven lines at 193.7, 226.1, 240.4, 295.98, 324.5, 340.1, 351.6, 358.24, 373.41, and 387.23 Å increase in intensity with respect to the 254.9 Å line with an increase in column length, reaching saturation value at a column length of 10^{21} cm^{-2}. The magnetic dipole transition $2p^5 3s(^3P_0 - ^1P_1)$ at 1153.2 Å is also enhanced by opacity.

Even though I(15.02)/I(17.10) and I(15.02)/I17.05) are sensitive to electron temperature they cannot be used for temperature diagnostic because of resonance scattering of the 15.02 Å line. Instead, Fe XVII X-ray lines in conjunction with Fe XVIII lines have been used for temperature diagnostics (Phillips et al. [40]). Atomic data and spectral line intensities

for the neon like isoelectronic sequence (Si V through Kr XXVII) have been calculated by Bhatia et al. [41] using $2s^2 2p^6$, $2s^2 2p^5 3s$, $2s^2 2p^5 3p$, and $2s^2 2p^5 3d$ configurations.

It is interesting to note that there are no other lines of comparable intensity as that of the line due to the transition $3d \rightarrow 2p$ in Fe XVII. Therefore, this line at 15 Å is one of the "benchmark" lines in X-ray astronomy.

8. Fe XV

Fe XV has X-ray lines in the range from 53.07 to 73.94 Å from an M-class solar flare. They have been observed by Acton et al. [42] with a high-resolution rocket-borne grazing incidence spectrograph telescope (XSST). Bhatia et al. [43] and Bhatia and Mason [44] carried calculations for 78 fine-structure levels using 13 configurations $3s^2$, $3s3p$, $3p^2$, $3s3d$, $3p3d$, $3s4s$, $3s4p$, $3s4d$, $3s4f$, $3p4s$, $3s4p$, $3s4d$, *and* $3p4f$.

Energy levels, transition rates, and collision strengths at incident electron energies of 25, 50, and 75 Ry were calculated. Statistical equations were solved for level populations to calculate intensity ratios at N_e (cm^{-3}) = 10^8, 10^9, 10^9, 10^{10}, 10^{11}, and 10^{12} and log (T_e) = 6.7. Some results for four transitions are given in Table 10.

Table 10. Collision strengths at 25, 50, and 75 Ry, and intensity ratios for four transitions in Fe XV are given.

Transition	Collision Strengths			Intensity
	25	50	75	
$3s^2\,{}^1S_0 - 3s4s\,{}^3S_0$	2.169 (−3)	8.830 (−4)	4.730 (−4)	
$3s^2\,{}^1S_0 - 3s4s\,{}^1S_0$	9.506 (−2)	1.054 (−1)	1.088 (−1)	
$3s4s\,{}^1S_0 - 3s3p\,{}^1P_1$	1.730 (−2)	3.646 (−2)	5.179 (−2)	3.88
$3s^2\,{}^1S_0 - 3s4p\,{}^1P_1$	1.052 (−2)	2.786 (−2)	4.457 (−2)	1.00

Collision strengths for the monopole transition $3s^2\,{}^1S_0 - 3s4s\,{}^1S_0$ are very large, resulting in appreciable level population of $3s4s$. This results in appreciable intensity of the dipole-allowed line $3s4s\,{}^1S_0 - 3s3p\,{}^1P_1$ at 69.74 Å, consistent with the observed intensity of the unidentified line at 69.444 Å.

The emission lines in Fe XV have been observed by SERTS in an active region on the Sun. The 13-configuration calculation of [43] did not include $3d^2$, which resulted in a poor representation of $3p^2\,{}^1S_0$ level. Therefore, Bhatia and Mason [44] calculated atomic data using configurations $3s^2$, $3s3p$, $3p^2$, $3s3d$, $3p3d$, *and* $3d^2$. Recently, Eissner et al. [45] has carried out an R-matrix calculation using exactly the same set of configurations. The two calculations agree so far as the energy levels and transition rates are concerned. A comparison between collision strengths at 50 Ry obtained in DW approximation and R-matrix approach, for a few transitions, is shown in Table 11, showing that DW results are reliable.

Table 11. Comparison of collision strengths in Fe XV obtained from DW and R-matrix calculations.

Transition	DW	R-Matrix
$3s^2\,{}^1S_0 - 3s3p\,{}^1P_1$	4.135	4.176
$3s3p\,{}^3P_0 - 3s3d\,{}^3D_1$	1.171	1.164
$3s3p\,{}^3P_2 - 3p^2\,{}^3P_2$	1.566	1.551
$3s3p\,{}^3P_2 - 3s3d\,{}^3D_3$	5.015	4.976
$3s3p\,{}^1P_1 - 3p^2\,{}^1S_0$	1.961	1.910

The contribution of resonances becomes less important at high temperatures. The level populations obtained using DW and R-matrix rates agree well. Using the DW atomic

data, we calculated the intensity ratios of various extreme-ultraviolet (EUV) lines in Fe XV at log (N_e) = 11, 12, and 13 cm^{-3} and compare them in Table 12 with those observed in active regions of the Sun by SERTS (Thomas and Neupert [23]).

Table 12. Comparison of calculated intensities at log (T_e) = 6.4 with observations.

Transitions	λ (Å)	Log (N_e)			
		Observed	11	12	13
$3s3d\,^1D_2 - 3s3p\,^1P_1$	243.780	7.21 (−2)	4.79 (−2)	4.79 (−2)	4.79 (−2)
$3s3p\,^1P_1 - 3s^2\,^1S_0$	284.158	1.000	1.000	1.000	1.000
$3p^2\,^3P_2 - 3s3p\,^3P_1$	292.251	5.78 (−3)	6.85 (−3)	6.85 (−3)	7.44 (−3)
$3p^2\,^3P_1 - 3s3p\,^3P_2$	321.782	4.68 (−3)	5.11 (−3)	5.11 (−3)	5.59 (−3)
$3p^2\,^1D_2 - 3s3p\,^3P_2$	327.030	1.16 (−2)	9.95 (−3)	9.95 (−3)	1.01 (−2)
$3s3d\,^3F_4 - 3s3d\,^3D_2$	372.758	2.14 (−2)	1.01 (−3)	1.10 (−3)	1.11 (−3)
$3s3p\,^1P_1 - 3s^2\,^1S_0$	417.245	4.48 (=2)	2.59 (−2)	2.58 (−2)	2.74 (−2)

The lines at 292.251 and 321.782 Å indicate a density of $N_e = 10^{11}$ cm^{-3}. It is found that lines at 284.16 and 417.26 Å are optically thick (Kastner and Bhatia [46]).

9. Fe X

There are three famous lines: the 'green line' at 5303 Å in Fe XIV, the 'yellow line' at 5694 Å in Ca XV, and the 'red line' at 6374 Å in Fe X in the Sun. The latter is a visible forbidden line in the ground configuration $3s^23p^5$ due to the transition $^2P_{1/2} - ^2P_{3/2}$. Strong EUV lines in Fe X have been observed in the solar spectrum of the full Sun obtained by Milinovsky and Herous [47] during a sounding rocket flight. Thomas and Neupert [23] identified lines at 257.26 and 345.72 Å as Fe X lines in the SERTS-89 flight. Other observations are of lines at 174.526, 175.265, 177.240, 184.534, 190.046, 220.862, and 257.246 Å from the SERTS-95 (Brosius et al. [48], and with improved calibration of lines at 174.5338 and 177.2477 (Brosius [49])). Bhatia and Doschek [50] calculated atomic data using configurations $3s^23p^5$, $3s3p^6$, $3s^23p^43d$, and $3s3p^53d$, giving rise to 54 fine-structure levels. Collision strengths were calculated at five incident energies: 9, 18, 27, 36, and 45 Ry, and up to the total angular momentum = 21. The level populations at log N_e = 8, 9, 10, 11, and 12 and log T_e = 6 K are calculated and then the intensity ratios of various lines are calculated, as indicated in Table 13.

Table 13. Level populations of the lowest five levels in Fe X.

Configuration	Level	Electron Density (cm^{-3})				
		10^8	10^9	10^{10}	10^{11}	10^{12}
$3s^23p^5$	$^2P_{3/2}$	0.983	0.912	0.708	0.600	0.585
	$^2P_{1/2}$	0.113 (−1)	0.435 (−1)	0.152	0.216	0.226
$3s3p^6$	$^2S_{1/2}$	0.213 (−10)	0.205 (−9)	0.187 (−8)	0.179 (−7)	0.178
	$^4D_{5/2}$	0.127 (−7)	0.137 (−6)	0.146 (−5)	0.124 (−4)	0.115 (−3)
	$^4D_{7/2}$	0.106 (−2)	0.843 (−2)	0.289 (−1)	0.318 (−1)	0.295 (−1)

Table 13 gives level populations of the lowest five levels. The line at 257.26 Å is a blend of two lines from the transitions $3p^43d(^4D_{7/2,5/2} \rightarrow {}_2P_{3/2})$ and Δ J = 2 transition is a magnetic quadrupole transition. Therefore, the $^4D_{7/2}$ level can get much more populated than the $^4D_{5/2}$ level, as indicated in Table 13. This is a good example of a metastable level.

10. Fe VIII

A number of Fe VIII spectral lines in the range from 130 to 190 Å have been observed under quiet solar conditions by a grazing-incidence spectrograph with a spectral resolution of 0.06 Å flown in Aerobee-200 rockets (Behring [13,51]). The lines at 185.221 and 187.247 Å have been observed from the SERTS-95 flight (Brosius et al. [48]). The line at 185.221 Å is blended with a Ni XVI line. Bhatia and Eissner [52] calculated atomic data using configurations $3p^6 3d$, $3p^5 3d^2$, $3p^6 4s$, $3p^6 4p$, and $3p^5 3d 4s$, giving rise to 73 fine-structure levels. Collision strengths are calculated at 10, 20, 30, 50, and 70 Ry and for total angular momentum L^T up to 33. Level populations and intensity ratios of various lines have been calculated at $\log N_e$ (cm^{-3}) = 8 to 14 and $\log T_e$ = 5.57.

It is found that the forbidden infrared line 5.447 μm line is a density sensitive line and is due to the transition $2p^5 3d(^2D_{5/2} - ^2D_{3/2})$. This line should be useful to determine properties of coronal magnetic fields by measuring the Zeeman effect or Faraday rotation. The observed lines at 168.170 and 168.546 Å are due to transitions $3p^5 3d^2\,^2D_{5/2} - 3p^6 3d\,^2D_{5/2}$, $3p^5 3d^2\,^2P_{3/2} - 3p^6 3d\,^2D_{5/2}$ and their observed intensity ratio is 12/7 = 1.7, which agrees with the calculated ratio 0.0991/0.0527 = 1.9 at $N_e = 10^8$ cm^{-3}. The observed line at 168.929 Å, due to the transition $3p^5 3d^2\,^2P_{1/2} - 3p^6 3d\,^2D_{3/2}$, has intensity comparable to that of the line at 168.546 Å but appears to be blended with a second-order line at 84.491 Å. The lines at 159.705, 168.929, 186.599, and 256.981 Å with respect to the line 168.175 Å are sensitive to electron density in the range $\log N_e$ (cm^{-3}) = 8 to 10. The intensity ratio of line 195.972 and 194.661 Å is sensitive to electron density in the same range.

11. Fe XX

Atomic data for Fe XX have been calculated by Mason and Bhatia [53] using $2s^2 2p^3$, $2s2p^4$, $2s^2 2p^2 3s$, and $2s^2 2p^2 3d$ configurations and calculated collision strengths at 80 Ry. These configurations give rise to lines in the X-ray region, which have recently been identified in solar spectra by McKenzie et al. [25] and Phillips et al. [26]. The electron density in solar flares is 10^{11} to 10^{12} cm^{-3}, and the electron temperature is 10^7 K. The strongest transition has a predicted wavelength of 12.82 Å. In Table 14, we give intensity ratios of a few transitions. We indicate that the indices 1, 4, 23, 24, 25, 33, 34, 35 refer to states from $2s^2 2p^3\,^4S_{3/2}$, $2s^2 2p^3\,^2P_{1/2}$, $2s^2 2p^2 3d\,^2P_{3/2}$, $2s^2 2p^2 3d\,^4F_{7/2}$, and $2s^2 2p^2 3d\,^2P_{1/2}$, respectively. We find that the observed and theoretical intensity ratios for 12.846 Å relative to 12.827 Å agree well, but, as indicated by Phillips et al. [26], the line at 12.812 Å is probably blended with a Ni XIX or a Ni XX line.

Table 14. Intensity ratios of the X-ray lines from Fe XX.

Transition	λ (Å)	Log (N_e (cm^{-3}))				
		11	**12**	**13**	**14**	**15**
23-1	13.051	0.229	0.229	0.235	0.251	0.291
24-1	12.969	0.092	0.093	0.097	0.116	0.142
25-3	13.240	0.171	0.171	0.208	0.305	0.445
33-1	12.827	1.000	1.000	1.000	1.000	1.000
34-4	13.238	0.068	0.069	0.0071	0.1089	0.112
35-1	12.812	0.440	0.440	0.438	0.442	0.450

12. Fe XXIII

Bhatia and Mason [54] calculated atomic data for Fe XXIII using configurations $2s^2$, $2s2p$, $2p^2$, $2s3s$, $2s3p$, and $2s3d$, giving rise to 20 fine structure levels. The level and energy values are given in Table 15. The observed UV wavelengths are taken from Lawson and Peacock [55].

Table 15. Levels and energy values (cm^{-1}).

Index	Configuration	Level	Energy	Observed
1	$2s^2$	$^1S_0$	0.0	0.0
2	2s2p	$^3P_0$	348.190	
3		$^3P_1$	380.485	379.100
4		$^3P_2$	471.927	
5		$^1P_1$	758.914	752.800
6	$2p^2$	$^3P_0$	956.966	956.200
7		$^3P_1$	1027.837	1027.400
8		$^3P_2$	1,076,089	1071.900
9		$^1D_2$	1,209,888	1204.600
10		$^1S_0$	430,417	1,422,900
11	2s3s	$^3S_1$	920,252	8,891,200
12		$^1S_0$	8,991,251	
13	2s3p	$^3P_0$	9,089,225	
14		$^3P_1$	9,088,907	9,076,000
15		$^3P_2$	9,121,415	
16		$^1P_1$	9,118,856	9,107,500
17	2s3d	$^3D_1$	9,213,076	9,181,100
18		$^3D_2$	9,217,883	9,181,100
19		$^3D_3$	9,225,493	
20		$^1D_2$	9,289,548	9,272,900

In Table 16, we give intensity ratios of strong UV and X-ray lines and compare them with observations. The intensity ratios are with respect to the transition $2s^2\,^1S_0 - 2s3p\,^1P_1\ (1-16)$ at $N_e = 10^9$ cm^{-3} and electron temperatures of 1.0, 1.3, and 2.0 $\times$ 10^7 K.

Table 16. Intensity ratios of UV and X-ray lines.

Transition	λ (Å)	Electron Temperature × 10^7		
i-j		1.0	1.3	2.0
3-1	263.76	0.396	0.258	0.135
4-3	1104	0.028	0.018	0.008
5-1	132.83	13.337	9.460	6.019
7-2	147.24	0.013	0.008	0.003
8-3	144.38	0.008	0.005	0.003
9-4	136.83	0.014	0.010	0.007
9-5	221.33	0.008	0.006	0.004
10-5	149.22	0.012	0.008	0.005
11-3	11.748	0.024	0.017	0.007
11-4	11.870	0.046	0.033	0.014
12-5	12.15	1.452	1.324	1.118
14-1	11.018	0.769	0.724	0.655
16-1	10.980	1.0	1.0	1.0
17-2	11.125	0.073	0.054	0.022
17-3 and 18-2	11.361	0.054	0.040	0.016
18-4	11.485	0.050	0.016	0.015
19-4	11.459	0.265	0.191	0.074
20-5	11.737	2.143	1.908	1.509

The strongest line is 132.83 Å in the solar flare spectra obtained by the Goddard Space Flight Center's grating spectrometer on OSO [56]. There is possibly a weak Fe XXIII blend at 132.85 Å (Bhatia and Mason [57]). The line at 263.76 Å has been studied from spectra obtained with the Naval Research Laboratory's spectrograph (171 − 630 Å) aboard Skylab (Widing [58]). A line at 11.7 Å, which is given as 117.737 Å in Table 16, has been identified in solar spectra as Fe XXIII [59].

13. Ni XV

Atomic data for Ni XV have been calculated by Landi and Bhatia [60] using $3s^23p^2$, $3s3p^3$, $3s^23p3d$, $3p^4$, $3s3p^23d$, $3s^23p4s$, $3s^23p4p$, $3s^23p4d$, and $3s^23p4f$ configurations, giving rise to 126 fine-structure levels. The highest level is $^1D_2$ of the configuration $3s^23p4f$ at an energy of 219,6753 cm^{-1}. Collision strengths are calculated at 7.8, 18.5, 33.5, 53.5, and 80.2 Ry. Electron temperature is logT_e (K) = 6.4, corresponding to the maximum abundance of Ni XV. Level populations are calculated for electron densities in the range 10^8–10^{14} cm^{-3}. Level populations for the first five levels at various densities are given in Table 17. The first five levels refer to $^3P_0$, $^3P_1$, $^3P_2$, $^1D_2$, and $^1S_0$ states of $3s^23p^2$ configuration.

Table 17. Level populations in Ni XV.

Key	Electron Density (cm^{-3})						
	10^8	10^9	10^{10}	10^{11}	10^{12}	10^{13}	10^{14}
1	9.997 (−1)	9.975 (−1)	9.752 (−1)	7.978 (−1)	3.155 (−1)	1.162 (−1)	8.726 (−2)
2	1.149 (−4)	1.146 (−3)	1.117 (−2)	8.880 (−2)	2.691 (−1)	2.804 (−1)	2.426 (−1)
3	1.384 (−4)	1.381 (−3)	1.352 (−2)	1.112 (−1)	3.809 (−1)	4.262 (−1)	3.818 (−1)
4	1.341 (−6)	1.349 (−5)	1.422 (−4)	1.988 (−3)	3.080 (−2)	1.573 (−1)	2.449 (−1)
5	4.212 (−8)	4.209 (−7)	4.177 (−6)	3.939 (−5)	3.613 (−4)	4.535 (−3)	2.228 (−2)

14. Mo VI to MO XIV

The Superstructure [3] and Distorted-wave [4] codes have been useful for diagnostics of the solar and astrophysical plasma but also proved useful to identify lines of molybdenum spectrum emitted in the Alcator tokamak in the range 300 to 550 Å [61].

15. Determination of Electron Temperature

Up to now, we have assumed that the electron temperature T_e is known from the ionization balance. However, it is possible to infer electron temperatures from temperature sensitive allowed lines when they are observed from the same ion and the lines do not differ much in wavelengths. For example, such lines are present in Mg II. Indicating $3s$, $3p$, and $3d$ levels by 1, 2, and 3, the intensity ratios of two emission lines from $3d \rightarrow 3p$ and $3p \rightarrow 3s$ in the absence of chromospheric radiation can be written as

$$\frac{I_{32}}{I_{21}} = \frac{\Delta E_{23} C_{23}}{\Delta E_{12} C_{12}} \propto \exp\left(\frac{\Delta E_{12} - \Delta E_{23}}{kT_e}\right) \tag{16}$$

This ratio is sensitive to T_e. Feldman and Doschek [62] analyzed the Mg II spectra recorded by the NRL normal-incident slit spectrograph on SKYLAB. These lines are emitted around 2800 Å within a few Å of each other. A comparison with observations indicates $T_e \leq 1.8 \times 10^4$ K in the quiet Sun and active regions. This is in agreement with the predicted temperature of formation of Mg II based on ionization equilibrium calculation of Jordan [63].

Up to now, we have described atomic data calculations of a few ions carried out using the Superstructure and Distorted-wave codes. There are many more ions for which data have been calculated, and it is not possible to discuss all that has been done. These data proved to be of great importance tosolar- and astro-physicists. The atomic data calculated at

Goddard were compiled into a database for diagnostic purposes. In 1985, the well-known astrophysicist Margaret Burbidge (1919–2020) visited the theoretical division and came to know about the database. She came to my room and asked me to show to her how the database can be used for a particular case. Her visit to my room was written in Goddard weekly! All the atomic data that have been calculated at Goddard are available in the CHIANTI database at the United States Naval Research Laboratory.

16. Conclusions

Among the large number of calculations carried out using the Superstructure and Distorted-wave codes, we have noted a few of these calculations. We have assumed a constant element abundance and steady state coronal equilibrium condition in the calculations of intensities of various emission lines. In general, the ionization and recombination processes are very slow compared to excitation processes. Therefore, a steady state condition can be assumed. Some of the high-lying levels can be populated by charge exchange and some levels can be populated by the dielectronic recombination of electrons with ions. We have not considered these processes. Fine-structure levels can be excited by proton impact as indicated by Kastner and Bhatia [64]. Excitation cross sections by proton impact have been included in many cases. Calculations carried out using codes [3,4] have been very helpful in identifying lines in observed solar spectra. The Distorted-wave calculations are reliable as shown in the case of Fe XV by the agreement of collision strengths calculated in the Distorted-wave and R-matrix formalism. The Superstructure and Distorted-wave calculations have proved to be reliable in analyzing the solar and astrophysical observations. All the calculated data are available in the CHIANTI database at NRL. There have been very, very few measurements of excitation cross sections like the one for S III [65] and, considering the need for the enormous atomic data required to analyze solar and astrophysical data, the recourse has been to calculate the required data.

There are no atomic data available using CCC and ICTF methods. Comparisons have been made in some cases, as indicated in Table 11, where the same atomic data were calculated using the R-matrix approach. It is possible to compare with a method like lose-coupling approach when a few results are involved, as has been done in the case of excitation of the 2S state of the atomic hydrogen [66].

The strength of these codes is that it is possible to calculate a large amount of atomic data without using enormous amount of computer time, which is very expensive. It would not be possible to work on many ions if too much funding was required. The drawback is that it is not possible to modify these codes. It is impossible to include resonance contribution in any particular case. These codes are very complicated and it took a few people to work out the theoretical and computational details. Over the year, whenever there were problems with the codes, help from Werner Eissner was sought.

Werner Eissner died on 6 April 2022. We will miss his sage advice. This paper is dedicated to him. Without his constant help, not much could have been achieved.

Funding: The research received no external funding.

Institutional Review Board Statement: Not applicable.

Informed Consent Statement: Not applicable.

Data Availability Statement: Not applicable.

Conflicts of Interest: There is no conflict of interest.

References

1. Neupert, W.M. Satellite lines in the solar X-ray spectrum. *Sol. Phys.* **1971**, *18*, 474–488. [CrossRef]
2. Bhatia, A.K.; Temkin, A. A distorted-wave methodology for electron-ion impact excitation: Calculation for two-electron ions. *J. Phys. B At. Mol. Phys.* **1977**, *10*, 2893. [CrossRef]
3. Eissner, W.; Jones, M.; Nussbaumer, H. Techniques for the calculation of atomic structures and radiative data including relativistic corrections. *Comput. Phys. Commun.* **1974**, *8*, 270–306. [CrossRef]

4. Eissner, W.; Seaton, M.J. Computer programs for the calculation of electron-atom cross sections. 1. General Formalism. *J. Phys. B* **1972**, *5*, 2187–2198. [CrossRef]
5. Mason, H.E.; Bhatia, A.K. Theoretical intensity ratios for the UV lines of Mg VII, Si IX, and S XI. *Mon. Not. R. Astron. Soc.* **1978**, *184*, 423–437. [CrossRef]
6. Bhatia, A.K.; Mason, H.E. Theoretical atomic structure and electron scattering data for ions in the nitrogen isoelectronic sequence: Mg VI, Si VIII, Ar XII, and Ca XIV. *Mon. Not. R. Astron. Soc.* **1980**, *190*, 925–929. [CrossRef]
7. Kelly, R.L.; Palumbo, L.J. *Atomic and Ionic Emission Lines below 2000 Å Hydrogen through Krypton*; Naval Research Laboratory: Washington, DC, USA, 1973; p. 7599.
8. Cook, J.W.; Keenan, F.P.; Bhatia, A.K. The allowed lines of O IV near 1340 Angstrom in high electron density solar flare. *Astrophys. J.* **1994**, *425*, 861. [CrossRef]
9. Bhatia, A.K.; Thomas, R.J. Atomic data and spectral line intensities for Mg VIII. *Astrophys. J.* **1998**, *497*, 483–492. [CrossRef]
10. Mason, H.E.; Doschek, G.A.; Feldman, U. Fe XXI as an electron density diagnostic in solar flares. *Astron. Astrophys.* **1979**, *73*, 74–81.
11. Bhatia, A.K.; Kastner, S.O. Collision strengths and transition rates for OIII. *At. Data Nucl. Data Tables* **1993**, *54*, 133–164. [CrossRef]
12. Bhatia, A.K.; Kastner, S.O.; Behring, W.E. The solar O III spectrum I. Photoexcitation of EUV lines by He II Lyman-alpha. *Astrophys. J.* **1982**, *257*, 887–895. [CrossRef]
13. Behring, W.E.; Cohen, L.; Feldman, U. The solar spectrum: Wavelengths and identifications from 60 to 385 Å. *Astrophys. J.* **1972**, *175*, 493–523. [CrossRef]
14. Vernazza, J.E.; Reeves, E.M. Extreme ultraviolet composite spectra of representative solar features. *Astrophys. J. Suppl. Ser.* **1978**, *37*, 485–513. [CrossRef]
15. Kastner, S.O.; Behring, W.E.; Bhatia, A.K. The solar O III spectrum. II. Longer wavelengths, line widths, and the He II Lyman α radiation field. *Astrophys. J. Suppl. Ser.* **1983**, *53*, 129–145. [CrossRef]
16. Bhatia, A.K.; Kastner, S.O. Measurement of the He II radiation field in planetary nebulae through Bowen fluorescence. *Phys. Scr.* **1987**, *35*. Available online: https://ntrs.nasa.gov/citations/19870059013 (accessed on 13 March 2022). [CrossRef]
17. Kastner, S.O.; Bhatia, A.K. On Bowen enhancement of the N III spectra under solar and nebular conditions. *Astrophys. J.* **1984**, *287*, 945–957. [CrossRef]
18. Kastner, S.O.; Bhatia, A.K. PAR: Photoexcitation by accidental resonance. *Comments At. Mol. Phys.* **1986**, *18*, 39.
19. Fawcett, B.C.; Jordan, C.; Lemen, J.R.; Phillips, K.J.H. New spectral line identifications in high-temperature flares. *Mon. Not. R. Astron. Soc.* **1987**, *225*, 1013–1023. [CrossRef]
20. Phillips, K.J.H.; Bhatia, A.K.; Mason, H.E.; Zarro, D.M. High coronal electron densities in a solar flare from Fe XXI and Fe XXII X-ray line measurements. *Astrophys. J.* **1996**, *466*, 549. [CrossRef]
21. Mason, H.E.; Storey, P.J. Atomic data for Fe XXII. *Mon. Not. R. Astron. Soc.* **1980**, *191*, 631–639. [CrossRef]
22. Bhatia, A.K.; Seely, J.F.; Feldman, U. Atomic data and spectral line intensities for carbon isoelectron sequence (Ar XIII through Kr XXXI). *At. Data Nucl. Data Tables* **1987**, *36*, 453–494. [CrossRef]
23. Thomas, R.J.; Neupert, W.M. Extreme ultraviolet spectrum of a solar active region from SERTS. *Astrophys. J. Suppl. Ser.* **1994**, *91*, 461–482. [CrossRef]
24. Bhatia, A.K.; Kastner, S.O. Multilevel calculation of the NE IV solar spectrumv. *Astrophys. J.* **1988**, *332*, 1063–1075. [CrossRef]
25. McKenzie, D.L.; Landecker, P.B.; Broussard, R.M.; Rugge, H.R.; Young, R.M.; Feldman, U.; Doschek, G.A. Solar flare X-ray spectra between 7.8 and 23.0 Angstrom. *Astrophys. J.* **1980**, *241*, 409–416. [CrossRef]
26. Phillips, K.J.L.; Fawcett, B.C.; Kent, B.J.; Gabriel, A.H.; Leibacher, J.W.; Wolfson, J.L.; Mason, H.E. Solar flare X-ray spectra from the Solar Maximum Mission Flat Crystal spectrometer. *Astrophys. J.* **1982**, *256*, 774–787. [CrossRef]
27. Bhatia, A.K.; Doschek, G.A. Atomic data and spectral line intensities for N_e-like Fe XVII. *At. Data Nucl. Data Tables* **1992**, *52*, 1–23. [CrossRef]
28. Feldman, U.; Doschek, G.A.; Seely, J.F. New identifications of Fe XVII spectral lines in solar flares. *Mon. Not. R. Astron. Soc.* **1985**, *212*, 41p–45p. [CrossRef]
29. Doschek, G.A.; Feldman, U.; Bhatia, A.K. Intensities of the neon-like iron (Fe^{+16}) $2p^5 3s - 2p^5 3s$ and $2p^5 3p - 2p^5 3d$ transitions in solar-flare spectra. *Phys. Rev. A* **1991**, *43*, 2565. [CrossRef]
30. Brown, G.V.; Beirersdorfer, P.; Leidahl, D.A.; Widman, K.; Kahn, S.M. Laboratory measurements and modelling of Fe XVII X-ray spectrum. *Astrophys. J.* **1998**, *502*, 1015–1026. [CrossRef]
31. Rugge, H.R.; McKenzie, D.L. X-ray line ratios for Fe XVII observed in the solar flares. *Astrophys. J.* **1985**, *297*, 338–346. [CrossRef]
32. Beiersdorfer, P.; Behar, E.; Boyce, K.R.; Brown, G.V.; Chen, H.; Gendreau, K.C.; Gu, M.F.; Gygax, J.; Kahn, S.M.; Kelley, R.L.; et al. laboratory measurements of the relative intensity of the 3*s*-3*p* and 3*d*-2*p* transitions in Fe XVII. *Astrophys. J.* **2002**, *576*, L169. [CrossRef]
33. Laming, J.M.; Kink, I.; Takacs, E.; Dorto, J.V.; Gillaspy, J.D.; Silver, E.H.; Schnopper, H.W.; Bandler, S.R.; Brickhouse, N.S.; Murray, S.S.; et al. Emission-line intensity ratios in Fe XVII obtained with a microcalorimeteron on an electron beam ion trap. *Astrophys. J.* **2000**, *545*, L161. [CrossRef]
34. Bernitt, S.; Brown, G.V.; Rudolph, J.K.; Steinbrugge, R.; Graf, A.; Leutenegger, M. An unexpected low oscillator strength as the origin of the emission problem. *Nature* **2012**, *492*, 225–228. [CrossRef] [PubMed]

35. Phillips, K.J.H.; Greer, C.J.; Bhatia, A.K.; Mason; Keenan, F.P. Active region electron density and dimensions from Fe XVII X-ray lines. *Astrophys. J.* **1996**, *369*, L57. [CrossRef]
36. Saba, J.L.R.; Schemlz, J.T.; Bhatia, A.K.; Strong, K.T. Fe XVII soft X-ray lines theory and data comparisons. *Astrophys. J.* **1999**, *519*, 1064. [CrossRef]
37. Kastner, S.O.; Kastner, R.E. Opacity ratios for Doppler-broadened lines from common upper levels. *J. Quant. Spectrosc. Radiat. Transf.* **1990**, *44*, 275–288. [CrossRef]
38. Kühn, S.; Cheung, C.; Oreshkina, N.S.; Steinbrügge, R.; Togawa, M.; Shah, C.; Bernitt, S.; Buck, J.; Hoesch, M.; Seltmann, J.; et al. Oscillator strength ratio of two Fe XVII soft X-ray transitions essential for diagnostics final agrees with theory. *arXiv* **2022**, arXiv:2201.09070k 2022.
39. Bhatia, A.K.; Kastner, S.O. The optically thick Fe XVII spectrum: X-ray, extreme ultraviolet, and forbidden line ratios. *Astrophys. J.* **1999**, *516*, 482–489. [CrossRef]
40. Phillips, K.J.H.; Greer, C.J.; Bhatia, A.K.; Coffey, I.H.; Barnsley, R.; Keenan, F.F. Fe XVII X-ray lines in solar coronal and laboratory plasmas. *Astron. Astrophys.* **1997**, *324*, 381–394.
41. Bhatia, A.K.; Feldman, U.; Seely, J.F. Atomic data and spectral line intensities for the neon isoelectronic sequence (Si V through Kr XXVii). *At. Data Nucl. Data Tables* **1985**, *32*, 435–469. [CrossRef]
42. Acton, L.W.; Bruner, M.E.; Brown, W.A.; Fawcett, B.C.; Schweizer, W.; Speer, R.J. Rocket spectrogram of a solar flare in the 10–100 Å region. *Astrophys. J.* **1985**, *291*, 865–878. [CrossRef]
43. Bhatia, A.K.; Mason, H.E.; Blancard, C. Atomic data and spectral line intensities for n = 3-3 and n = 3-4 X-ray transitions in Fe XV. *At. Data Nucl. Data Tables* **1997**, *66*, 83–117. [CrossRef]
44. Bhatia, A.K.; Mason, H.E. Spectral line intensities for n = 3-3 EUV transitions in Fe XV. *At. Data Nucl. Data Tables* **1997**, *66*, 119–128. [CrossRef]
45. Eissner, W.; Galavis, M.E.; Mendoza, C.; Zippen, C.J. Atomic data from Iron project XXXVIII. Electron impact excitation of the fine-structure transitions in the n = 3 complex of Fe XV. *Astron. Astrophys. Suppl. Ser.* **1999**, *137*, 165–173. [CrossRef]
46. Kastner, S.O.; Bhatia, A.K. Optically thin and thick Fe XV spectrum: Effect of self-absorption in the 284.16 Å resonance line. *Astrophys. J.* **2001**, *553*, 421–428. [CrossRef]
47. Milinovsky, M.; Heroux, L. An analysis of the solar exteme ultraviolet between 50 and 300 Å. *Astrophys. J.* **1973**, *181*, 1009–1030. [CrossRef]
48. Brosius, J.W.; Davila, J.M.; Thomas, R.J. Solar active region and quiet-sun extreme ultraviolet spectra from SERTS-95. *Astron. Astrophys. Suppl. Ser.* **1998**, *119*, 255–276. [CrossRef]
49. Brosius, J.W.; Thomas, R.J.; Davila, J.M. SERTS-95 measurements of wavelength shifts in coronal emission lines across a solar active region. *Astrophys. J.* **1999**, *526*, 494. [CrossRef]
50. Bhatia, A.K.; Doschek, G.A. Atomic data and spectral line intensities for Fe X. *At. Data Nucl. Data Tables* **1995**, *60*, 97. [CrossRef]
51. Behring, W.E.; Cohen, L.; Feldman, U.; Doschek, G.A. The solar spectrum: Wavelengths and identifications from 160 to 770 Angstrom. *Astrophys. J.* **1976**, *203*, 521–527. [CrossRef]
52. Bhatia, A.K.; Eissner, W. Atomic data and spectral line intensities for Fe VIII. *At. Data Nuclear Data Tables* **2000**, *76*, 270–346. [CrossRef]
53. Mason, H.E.; Bhatia, A.K. Atomic calculations for the Fe XX X-ray lines. *Astron. Astrophys. Suppl. Ser.* **1983**, *52*, 181–192.
54. Bhatia, A.K.; Mason, H.E. Atomic calculations for Fe XXIII, UV, and X-ray lines. *Astron. Astrophys.* **1981**, *103*, 324–330.
55. Lawson, K.D.; Peacock, N.J. The analysis of the n = 2-2 transitions in XUV spectra of Cr to Ni. *J. Phys. B Atom. Mol. Phys.* **1980**, *13*, 3313. [CrossRef]
56. Kastner, S.O.; Neupert, W.M.; Swartz, M. Solar-flare emission lines in the range from 66 to 171 Å, $2s^r2p^k - 2s^{r-1}2p^{k+1}$ transition in highly ionized iron. *Astrophys. J.* **1974**, *191*, 261–270. [CrossRef]
57. Bhatia, A.K.; Mason, H.E. Atomic calculations for the highly ionized iron ions produced in solar flares. In Proceedings of the Eighth International Colloquium on Ultraviolet and X-ray Spectroscopy of Astrophysical and Laboratory Plasmas, IAU Colloq. 86, Washington, DC, USA, 27–29 August 1984; Naval Research Laboratory: Washington, DC, USA, 1984; p. 141.
58. Widing, K.G. Fe XXIII 263 Å and Fe XXIV 255 Å emission in solar flares. *Astrophys. J.* **1975**, *197*, L33. [CrossRef]
59. Neupert, W.M.; Swartz, M.; Kastner, S.O. Solar flare line emission between 6 Å and 25 Å. *Sol. Phys.* **1973**, *31*, 171–195. [CrossRef]
60. Landi, E.; Bhatia, A.K. Atomic data and spectral line intensities for Ni XV. *At. Data Nucl. Data Tables* **2012**, *98*, 862–893. [CrossRef]
61. Finkenthal, M.; Bell, R.E.; Moos, H.W.; Bhatia, A.K.; Marmar, E.S.; Terry, J.L.; Rice, J.E. The molybdenum spectrum emitted by a Tokamak plasma in the 300–550 Å range. *Phys. Lett. A* **1981**, *82*, 123–126. [CrossRef]
62. Feldman, U.; Doschek, G.A. The 3s-3p and 3p-3d lines in Mg II observed above the solar limb from SKYLAB. *Astrophys. J.* **1977**, *212*, L147–L150. [CrossRef]
63. Jordan, C. The ionization equilibrium of elements between carbon and nickel. *Mon. Not. R. Astron. Soc.* **1969**, *142*, 501–521. [CrossRef]
64. Kastner, S.O.; Bhatia, A.K. Approximations for proton excitation: Erratum and extension. *Astron. Astrophys.* **1979**, *71*, 211–213.
65. Smith, S.J.; Greenwood, J.B.; Chatjain, A.; Tayal, S.S. Electron excitation cross sections for the 3s23p2 3P $\rightarrow$ 3s3p3 5So Transition in S^{2+}. *Astrophys. J.* **2008**, *541*, 501. [CrossRef]
66. Bhatia, A.K. Excitation of the 2*S* state of atomic hydrogen by electron impact. *Atoms* **2016**, *6*, 7. [CrossRef]